International Journal of Heat and Mass Transfer 64 (2013) 680–688

Contents lists available at SciVerse ScienceDirect

International Journal of Heat and Mass Transfer

journal homepage: www.elsevier.com/locate/ijhmt

Superadiabatic radiant porous burner with preheater and radiation corridors

Vahid Vandadi [a], Chanwoo Park [a,*], Massoud Kaviany [b]

[a] Department of Mechanical Engineering, University of Nevada, Reno, NV 89557-0312, USA
[b] Department of Mechanical Engineering, University of Michigan, Ann Arbor, MI 48105, USA

ARTICLE INFO

Article history:
Received 12 April 2013
Accepted 20 April 2013

Keywords:
Superadiabatic
Radiant burner
Porous media
Heat recirculation
Preheating
Pre-mixed
Lean combustion

ABSTRACT

The current efficiency of monolithic (including two-layer) radiant porous burners is less than 25% and here we introduce a novel structure for effective preheating and radiation routing to increase the efficiency. This recovers the flue gas heat to increase the inlet air temperature and raises the flame temperature locally above the adiabatic temperature (superadiabatic flame) for the fuel-lean conditions. The heat from the superadiabatic region is then extracted and conducted through embedded, high-thermal conductivity radiation corridors and is radiated, at a higher temperature than the flue gas, to the target. The analyses of local thermal non-equilibrium among the gas phase, two-layer porous solid, preheating heat exchanger, and radiant corridor are presented for the zeroth-order reaction of premixed methane/air. Radiant burner efficiency over 45% is predicted.

1. Introduction

Porous burners have been extensively studied because of their low pollutant emissions and fuel flexibility. The idea of the porous burner was initiated to find a simple way to produce a superadiabatic flame by inserting a high conductivity porous solid into the flame region to recuperate the heat of the hot downstream gas to cold upstream gas through the solid. Since the porous burners internally recirculate the combustion heat through convection, solid conduction, and radiation to preheat the incoming cold gas flow; they can operate at lower equivalence ratios of fuel/air mixture at higher flame speeds than the laminar flame.

The one-layer porous burners and multiple layers were studied by various researchers [1–5]. The porous burner made of three layers was numerically analyzed by Yoshizawa et al. [1]. In the study, the reaction was assumed to entirely take place in the middle layer. They reported that the temperature profiles were greatly affected by the interstitial heat transfer coefficient and radiation properties such as absorption coefficient, and optical thickness of the porous media. An experimental investigation was presented by Younis and Viskanta [6] to characterize the heat transfer between the gas and solid phases in a porous medium. A heat transfer correlation for different ceramic foams was presented.

The radiative heat transfer in the porous burners plays an important role in the recuperation of the combustion heat [7–11]. The effect of the solid thermal conductivity on the radiative heat transfer in packed beds was reported by Singh and Kaviany [7]. It was reported that the radiant conductivity was strongly influenced by the thermal conductivity of the solid phase and the emissivity of the particles. It was also reported that the sensitivity of the radiant conductivity with respect to the porosity was not significant. The local volume averaged method used in various studies of the combustion in porous media [12–15], is the two-medium treatment which allows a non-thermal equilibrium between the solid and gas phases. Sahraoui and Kaviany [12] presented a comparison of the direct simulation and volume averaged treatment of the premixed flame in a porous medium.

In recent years the porous burner using two-layer porous media with distinctively different thermophysical properties has been studied by many researchers to anchor the flame at the interface between two porous layers [16,17]. An experimental investigation on stabilization of flame using a two-layer porous burner made of randomly packed spherical alumina pellets was performed by Bubnovich et al. [16]. The results of the temperature profiles and pollutant emissions were reported for the equivalence ratios of 0.6 and 0.7 of methane/air mixture.

Several studies have utilized various burner designs to recover the heat loss of the exhaust gas to preheat the incoming fuel/air mixture [18–21]. The preheating effect on superadiabatic combustion of propane/air mixture was studied by Huang et al. [18]. They

* Corresponding author. Address: Department of Mechanical Engineering, University of Nevada, Reno, 1664 N. Virginia Street, Reno, NV 89557-0312, USA. Tel.: +1 775 682 6301; fax: +1 775 784 1701.
E-mail address: chanwoo@unr.edu (C. Park).

0017-9310/$ - see front matter © 2013 Elsevier Ltd. All rights reserved.
http://dx.doi.org/10.1016/j.ijheatmasstransfer.2013.04.054

Nomenclature

A	surface area (m^2)
A_{gs}/V	specific volume (1/m), ε/D_p
a_r	pre-factor of combustion reaction (1/s)
C	coefficient or thermal capacity (J/K)
c_p	specific heat of gas mixture (J/kg K)
C_r	thermal capacity ratio, C_{min}/C_{max}
D_g	species diffusivity (m^2/s)
D	diameter (m)
D^d_{xx}	thermal diffusivity due to dispersion (m^2/s)
$D^d_{m_{xx}}$	species diffusivity due to dispersion (m^2/s)
H	height (m)
h_h	heat transfer coefficient of the hot stream of the preheater (W/m^2 K)
I	modified Bessel, first kind
K	modified Bessel, second kind
k	thermal conductivity (W/m K)
L	length (m)
Le	Lewis number,$(k_{g,e}/(\rho c_p)_g)/D_{g,e}$
MW	molecular weight (kg/kmol)
$\dot{m}$	mass flow rate (kg/s)
$Nu_{D,p}$	Nusselt number, $h_v D_p^2/k_g$
N	number of components
NTU	number of transfer unit
$\dot{n}_{g,r,F}$	rate of consumption of fuel (kg/m^3 s)
P	pressure (Pa)
Pe	Peclet number, $\rho_g c_p \varepsilon u_g D_p/k_g$
Pr	Prandtl number
Q	rate of energy transfer (W)
q	heat flux (W/m^2)
R	radius (m)
r	radial coordinate (m)
Re	Reynolds number, $\rho_g \varepsilon u_g D_p/\mu$
R_g	universal gas constant (J/kmol K)
T	temperature (K)
U	overall heat transfer coefficient (W/m^2 K)
u	velocity (m/s)
X_F	flame location (m)
x	coordinate (m)
Y	mass fraction of species
y	coordinate (m)
W	width (m)
w_f	half thickness of fin (m)

Greek letters

α_g	thermal diffusivity (m^2/s)
ΔE_a	activation energy (J/kmol)
$\Delta h_{r,F}$	standard heat of reaction (J/kg)
ΔL	spacing of adjacent nodes (m)
ε	porosity or effectiveness
ε_r	emissivity
η	thermal efficiency (%)
μ	viscosity (Pa s)
ρ	density (kg/m^3)
σ_e	extinction coefficient (1/m)
σ_{PH}	ratio of free flow area and front area in preheater
σ_{SB}	Stefan–Boltzmann constant (W/m^2 K^4)
ϕ	equivalence ratio, $(\rho_{F,g}/\rho_g)/(\rho_{F,g}/\rho_g)_{stoich}$

Subscripts

a	actual or activation
ad	advection or adiabatic
air	air
ave	average
b	base of fin
c	cold stream
cb	combustion
cd	conduction
cv	convection
e	effective
F	fuel or flame
f	fins of radiation rods
g	gas phase
gs	gas to solid
h	hot stream or hydraulic
i	x-directional nodal index
in	inlet
ins	insulation
j	y-directional nodal index
max	maximum
min	minimum
o	out or oxygen
PH	preheater
PM	porous medium
p	pore or particle
RR	radiation rod
r	radiation or reaction
rad	radiation
rf	rod and fin
rs	radiating surface
s	solid phase
$stoich$	stoichiometric
t	target or total
tu	preheater tube
v	volumetric
xx	x-directional

Superscripts

d	dispersion
m	exponent or coefficient
$*$	normalized

Others

∞	ambient or surrounding

reported that the preheating had a great influence on ignition and extinction of flame. It was also shown that the decrease of the preheating equivalence ratio would increase the critical preheating energy to sustain a stable combustion mode.

In this paper, a novel porous radiant burner using a preheater and radiation corridors for high efficiency radiant output, is analyzed and the results from the numerical analysis using a zeroth-order combustion reaction model for methane/air mixture and non-thermal equilibrium formulation are presented.

2. Numerical analysis

The radiant porous burner considered for a numerical analysis is shown in Fig. 1(a) and (b) and consists of two-layer porous media (PM1, and PM2), a preheater (PH) and radiation rods (RR). The cold inlet air is heated by the preheater using hot flue gas from the porous burner. The preheated air is then mixed with the cold gaseous fuel flow in the upstream porous medium (PM1) with a fine porous structure. The downstream porous medium (PM2) with

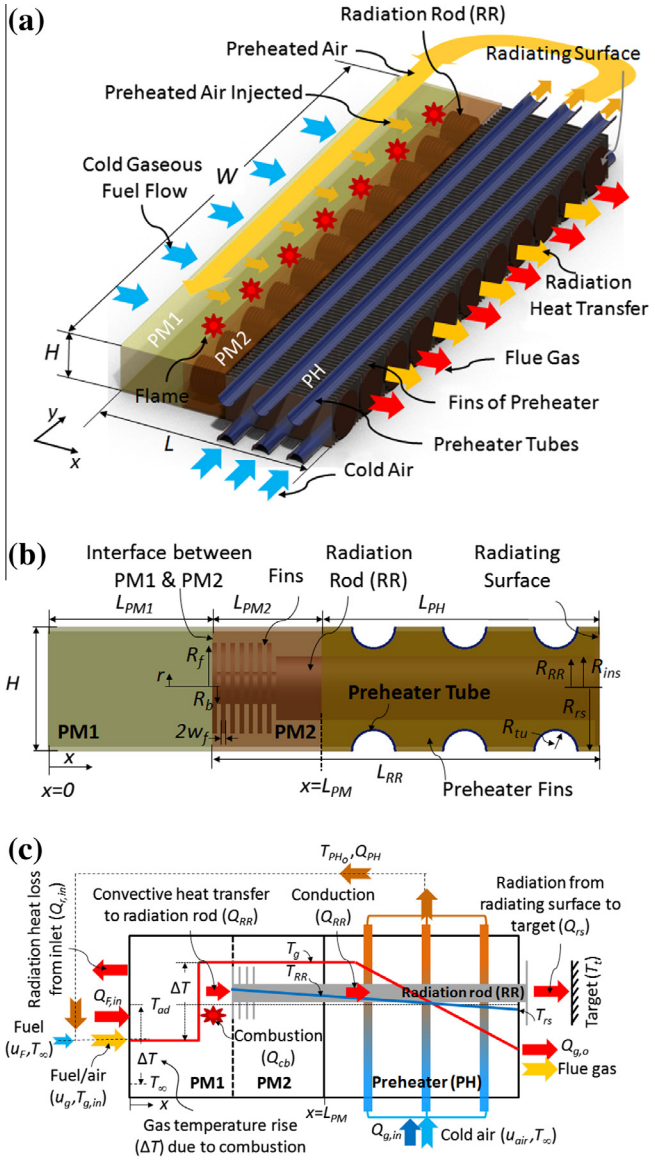

Fig. 1. (a) Schematic of the superadiabatic radiant porous burner with two-layer porous media, a preheater and radiation rods showing gas flows and heat transfers, (b) side view of computational domain, (c) schematic diagram of the superadiabatic radiant burner system showing heat transfer, mass flow and key temperatures.

a coarse porous structure serves as a flame holder to stabilize the flame where the fins of the radiation rods are located (Fig. 1(c)).

The heat transfers and mass flow in the superadiabatic radiant burner system are shown in Fig. 1(c). The combustion heat is extracted by the fins of the radiation rods (RR) and then conducted through the radiation rods to the radiating surfaces. The radiation rods made of a metallic material provide highly conducting paths from the flame to the radiating surfaces. The radiation rods are assumed to be coated with a low thermal conductivity material (thermal insulator) to reduce the heat loss to the colder surrounding flue gas being cooled by the preheater. Therefore, the combustion heat is efficiently transferred to the radiating surface at higher temperatures than the exiting flue gas temperature. As a result, the superadiabatic radiant burner can achieve higher thermal efficiency than the conventional burner.

Table 1
Thermophysical properties and dimensions of the superadiabatic radiant burner and coefficients of zeroth-order reaction model.

Burner dimensions			
Height, H (cm)			2.54
Length, L (cm)			12.1
Width, W (cm)			30.0
Porous media	PM1		PM2
Length, L_{PM} (cm)	3.6		2.4
Particle diameter, D_P (mm)	0.29		1.52
Porosity, ε	0.835		0.87
Emissivity, ε_r	1		1
Thermal conductivity, k_s (W/m K)	0.2		0.1
C	0.638		0.146
m	0.42		0.96
Radiation rod and fins of radiation rod			
Material	Carbon steel	L_{RR} (cm)	8.5
Melting point (K)	1750–1850	N_f	7
k_{RR} (W/m K)	50	R_f (cm)	1.0
k_{ins} (W/m K)	0.05	R_b (mm)	2.0
R_{RR} (cm)	0.7	R_{rs} (cm)	1.2
R_{ins} (cm)	0.75	w_f (mm)	0.5
Preheater			
L_{PH} (cm)			6.1
Tube radius, R_{tu} (mm)			5.1
Fin pitch (m^{-1})			314
Flow passage hydraulic diameter, D_h (mm)			3.63
Fin thickness (mm)			0.33
Free flow area/front area, σ_{PH}			0.534
Heat transfer area/total volume (m^2/m^3)			587
Fin area/total area			0.913
Number of preheater tubes, N_{tu}			3
Fuel, methane (CH_4)			
MW (kg/kmol)			16
$(\rho_{F,g}/\rho_g)_{stoich}$			1/18.12
$-\Delta h_{r,F}$ (J/kg) (HHV)			55.53×10^6
Reaction model coefficients			
a_r (1/s)			4.8×10^8
ΔE_a (J/kmol)			1.3×10^8

2.1. Porous burner

The porous burner consisting of upstream (PM1) and downstream (PM2) porous media as shown in Fig. 1(b) is analyzed using non-thermal equilibrium formulation. The thermophysical properties and dimensions of the burner system are presented in Table 1.

The conservation equations of mass, gas species, and energy for gas and solid phases of the porous burner are given by

$$\frac{\partial}{\partial x}(\varepsilon\rho_g u_g) = 0, \tag{1}$$

$$\varepsilon\rho_g u_g \frac{\partial Y_{F,g}}{\partial x} = \frac{\partial}{\partial x}\left(\rho_g D_{g,e}\frac{\partial Y_{F,g}}{\partial x}\right) + \varepsilon\dot{n}_{g,r,F}, \tag{2}$$

$$\varepsilon(\rho c_p u)_g \frac{\partial T_g}{\partial x} = \frac{\partial}{\partial x}\left(k_{g,e}\frac{\partial T_g}{\partial x}\right) + \mathrm{Nu}_{D,p}\frac{k_g}{D_p}\left(\frac{A_{gs}}{V}\right)(T_s - T_g) + \varepsilon\dot{n}_{g,r,F}\Delta h_{r,F}, \tag{3}$$

$$0 = \frac{\partial}{\partial x}\left(k_{s,e}\frac{\partial T_s}{\partial x}\right) + \mathrm{Nu}_{D,p}\frac{k_g}{D_p}\left(\frac{A_{gs}}{V}\right)(T_g - T_s). \tag{4}$$

The continuity, species and energy equations are discretized using finite volume method over the computational domain of the porous media (PM1 and PM2).

The density of the gas flow is computed from the ideal gas law, in which the properties of the gas mixture are considered and is given by

Table 2
Coefficients of the polynomial curvefit equations for the specific heat capacity and thermal conductivity of the gas phase [25].

	$c_1T^4 + c_2T^3 + c_3T^2 + c_4T + c_5$	
	$c_{p,g}$	k_g
c_1	1.3958×10^{-10}	2.930×10^{-14}
c_2	-6.5412×10^{-7}	-1.3208×10^{-10}
c_3	0.0010395	2.0396×10^{-7}
c_4	−0.44833	-6.4181×10^{-5}
c_5	1066.2	0.033158

$$\rho_g = \frac{P_g}{R_g T_g}. \tag{5}$$

The interstitial convective heat transfer is modeled by the volumetric Nusselt number [6] and is given by

$$\mathrm{Nu}_{D,p} = C\mathrm{Re}^m, \tag{6}$$

where C and m values are listed in Table 1. Re is the Reynolds number of the gas flow in the porous media and is given by

$$\mathrm{Re} = \varepsilon \rho_g u_g D_p/\mu. \tag{7}$$

The specific volume of the porous media is given by

$$A_{gs}/V = \varepsilon/D_p. \tag{8}$$

The effective thermal conductivity of the gas phase consists of diffusion and dispersion terms and is given by

$$k_{g,e} = \varepsilon k_g + (\rho c_p)_g D^d_{xx}, \tag{9}$$

where the thermal diffusivity [22] is given by

$$D^d_{xx} = 0.5\alpha_g \mathrm{Pe}, \tag{10}$$

and the Peclet number is given by

$$\mathrm{Pe} = \rho_g c_p \varepsilon u_g D_p/k_g. \tag{11}$$

The Lewis number is assumed to be unity as below,

$$\mathrm{Le} = \frac{k_{g,e}/(\rho c_p)_g}{D_{g,e}} = 1, \tag{12}$$

where the mass diffusivity is given by

$$D_{g,e} = \varepsilon D_g + D^d_{m_{xx}}. \tag{13}$$

The effective thermal conductivity of the solid phase consists of the volume-averaged thermal conductivity and the radiative thermal conductivity of the solid phase and is given by

$$k_{s,e} = (1-\varepsilon)k_s + \varepsilon k_{s,r}, \tag{14}$$

where the radiative thermal conductivity is given by

$$k_{s,r} = \frac{16\varepsilon_r \sigma_{SB} T_s^3}{3\sigma_e}. \tag{15}$$

The zeroth-order reaction rate is used to model the combustion of fuel/air mixture and is given by

$$\dot{n}_{g,r,F} = -a_r e^{-\Delta E_a/R_g T_g}, \tag{16}$$

where the coefficients of the combustion model (a_r and ΔE_a) for premixed methane/air flow are listed in Table 1.

Since the specific heat capacity and thermal conductivity of the gas phase significantly vary with temperature, they are given as the functions of temperature by fourth-order polynomial equations listed in Table 2.

The perfect mixing of the preheated air and fuel is assumed at the inlet of the burner. The equivalence ratio of the fuel/air mixture is defined as $\phi = (\rho_{F,g}/\rho_g)/(\rho_{F,g}/\rho_g)_{stoich}$. The velocity of the fuel/air mixture (u_g), entering the burner, is calculated by the mass conservation equation which is given by

$$\rho_g u_g HW\left[1 - \phi(\rho_{F,g}/\rho_g)_{stoich}\right] = N_{tu}\rho_{air} u_{air} \pi R^2_{tu} \tag{17}$$

The boundary conditions for the energy and species equations are presented below.

Inlet ($x = 0$):

$$-(1-\varepsilon)k_s \frac{\partial T_s}{\partial x} = \varepsilon_r \sigma_{SB}(T_s^4 - T_g^4), \tag{18}$$

$$T_g = T_{g,in}, \tag{19}$$

$$Y_{F,g} = \phi\left(\frac{\rho_{F,g}}{\rho_g}\right)_{stoich}. \tag{20}$$

Outlet ($x = L_{PM}$):

$$-(1-\varepsilon)k_s \frac{\partial T_s}{\partial x} = \varepsilon_r \sigma_{SB}(T_s^4 - T^4_{PH,ave}), \tag{21}$$

$$\frac{\partial T_g}{\partial x} = 0, \tag{22}$$

$$\frac{\partial Y_{F,g}}{\partial x} = 0. \tag{23}$$

It is assumed that the porous burner exchanges radiation heat at the outlet with the preheater at its average temperature. All the properties used for the numerical analysis are evaluated based on the mass-averaged mixture of air and fuel.

The governing equations of the porous burner are discretized using uniform grid nodes. The equations are solved by enough iteration until a convergence is achieved. The continuity equation of the gas flow, Eq. (1) is directly used to calculate the velocity at each node. The density of the gas flow is computed by ideal gas law. The initial temperature profiles for gas and solid phases with their peak temperatures at the interface of the upstream and downstream porous media are set to ignite the flame. Note that all properties are smoothed near the interface of two porous media to avoid numerical errors due to discontinuous properties. But the porosity of the porous media was allowed to vary across the interface (Eq. (4)).

2.2. Radiation rods and preheater

The radiation rods and preheater analyzed in this study are shown in Figs. 1(b) and 2. The radiation rod consists of (i) the radial fins located close to the interface of the two layers of the porous media, (ii) a stem and (iii) a radiating disk. The thermophysical properties and dimensions of the radiation rod and preheater are listed in Table 1.

The radial fins of the radiation rods are modeled by considering the convection and conduction heat transfers [23]. The equations and boundary conditions are given by

$$\frac{d}{dr}\left(r\frac{dT}{dr}\right) = \frac{r\mathrm{Nu}_{D,p}}{w_f(A_{gs}/V)D_p^2}(T - T_g), \tag{24}$$

$$T = T_b \quad \text{at } r = R_b, \tag{25}$$

$$\frac{dT}{dr} = 0 \quad \text{at } r = R_f, \tag{26}$$

where w_f is the half thickness of each fin.

The convection heat transfer is considered for the radial fins with an insulated tip boundary condition. The stem of the radiation rod is divided to as many nodes as aligned with the preheater tubes

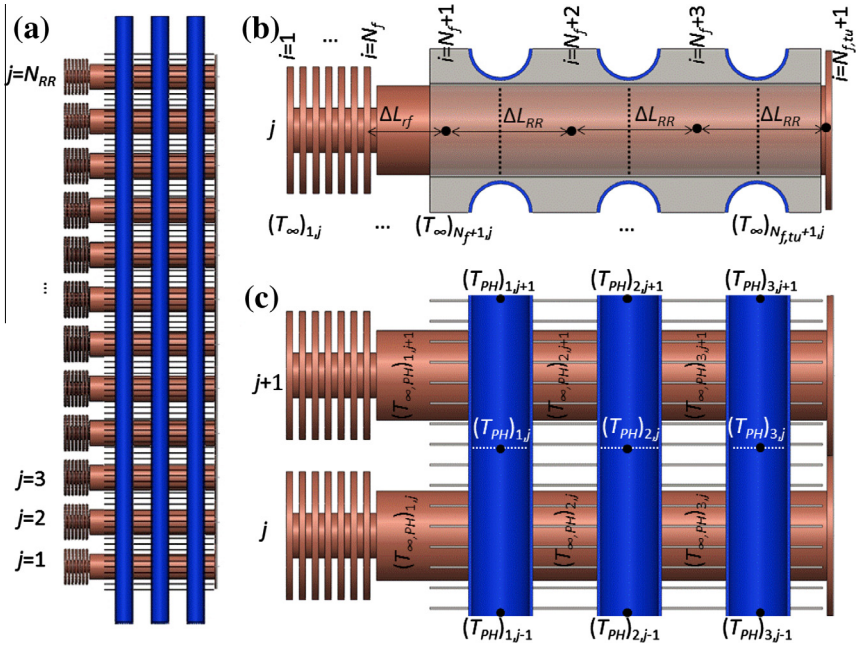

Fig. 2. (a) Top view of the preheater and radiation rods. (b) Side view of the radiation rods and preheater tubes showing a grid system of the radiation rods. (c) Magnified top view of the preheater tubes showing a grid system of the preheater tubes.

as shown in Fig. 2(b). The axial conduction only in the stem is considered because of the small temperature gradient in the radial direction. The radiation boundary condition is used at the radiating surface of the radiation rods.

The energy equations of the stem of the finned section of the radiation rods shown in Fig. 2(b) are given by

$$-4R_{RR}w_fC_fk_{RR}[T_{i,j}-(T_\infty)_{i,j}]+\frac{k_{RR}}{\Delta L_f}R_{RR}^2(T_{i+1,j}+T_{i-1,j}-2T_{i,j})=0,\quad i=1,\ldots,N_f, \tag{27}$$

where

$$C_f=\frac{m[K_1(R_bm)I_1(R_fm)-K_1(R_fm)I_1(R_bm)]}{K_0(R_bm)I_1(R_fm)+K_1(R_fm)I_0(R_bm)}, \tag{28}$$

where $m=\{\mathrm{Nu}_{D,p}k_g/[(A_{gs}/V)D_p^2k_{RR}w_f]\}^{\frac{1}{2}}$ and perfect insulation is assumed as the boundary condition for the first node ($i=1$), i.e., $T_{0,j}=T_{1,j}$

It is assumed that the presence of the radiation rods embedded in the downstream porous medium (PM2) do not affect the combustion occurring in the upstream porous medium (PM1). However, the specific volume of the downstream porous medium (PM2), A_{gs}/V is corrected considering the presence of the radiation rods and fins. Note that the burner is modeled as a one-dimensional system while the radiation rods and fins are modeled as two-dimensional systems.

The energy balance of the gas flow in the finned section of the radiation rods is given by

$$\dot{m}_hc_{p,h}[(T_\infty)_{i,j}-(T_\infty)_{i+1,j}]+4\pi R_{RR}w_fC_fk_{RR}[T_{i,j}-(T_\infty)_{i,j}]=0,\quad i=1,\ldots,N_f. \tag{29}$$

The unfinned section of the radiation rod is assumed to be insulated to reduce the heat loss to the surrounding gas flow and its energy equations are given by

$$\pi R_{RR}^2k_{RR}\left[\frac{T_{i+1,j}-T_{i,j}}{\Delta L_{RR}}-\frac{T_{i,j}-T_{i-1,j}}{\Delta L_{rf}}\right]-C_{ins}[T_{i,j}-(T_\infty)_{i,j}]=0,\quad i=N_f+1, \tag{30}$$

$$\pi R_{RR}^2k_{RR}\left[\frac{T_{i+1,j}+T_{i-1,j}-2T_{i,j}}{\Delta L_{RR}}\right]-C_{ins}[T_{i,j}-(T_\infty)_{i,j}]=0,\quad i=N_f+2,\ldots,N_{f,tu}, \tag{31}$$

$$-\pi R_{RR}^2k_{RR}\left[\frac{T_{i,j}-T_{i-1,j}}{\Delta L_{RR}}\right]-C_{ins}[T_{i,j}-(T_\infty)_{i,j}]=\varepsilon_rA_{rs}\sigma_{SB}T_{i,j}^4-\varepsilon_rA_t\sigma_{SB}T_t^4,\quad i=N_{f,tu}+1, \tag{32}$$

where

$$C_{ins}=\frac{2\pi\Delta L_{RR}}{\left[\frac{\ln(R_{ins}/R_{RR})}{k_{ins}}+\frac{1}{R_{ins}h_h}\right]}, \tag{33}$$

where the heat transfer coefficient is defined by the correlation of an appropriate compact heat exchanger and is given by

$$h_h=0.1566\left(\frac{\dot{m}_hD_h}{\sigma_{PH}HW\mu}\right)^{-0.389}\frac{\dot{m}_hc_{p,h}}{\sigma_{PH}HW\mathrm{Pr}_h^{2/3}}. \tag{34}$$

and T_t is the temperature of a target (heat sink).

The convective heat transfers between the flue gas, the radiation rod and the preheater are calculated in two steps. First the convective heat transfer to the radiation rod is calculated using the flue gas temperature, T_∞ by Eq. (27) and Eqs. (30)–(32). Then the reduced flue gas temperature, $T_{\infty,PH}$ is used to calculated the energy conservation equations of the flue gas flow which is given by

$$\dot{m}_hc_{p,h}[(T_\infty)_{N_f+i,j}-(T_{\infty,PH})_{i,j}]+C_{ins}[T_{N_f+i,j}-(T_\infty)_{i,j}]=0,\quad i=1,\ldots,N_{tu}. \tag{35}$$

The heat transfer in the preheater tubes is modeled by ε-NTU method in which each tube is considered separately and the tube length is also divided into small nodes to be aligned with the radiation rods as shown in Fig. 2(c). The flow configuration of the preheater corresponds to the case where the air flow inside the preheater tubes is unmixed and the flue flow is mixed and the effectiveness of the preheater is given by

Table 3
Stable range of the operation of conventional porous burner.

Φ	0.60	0.65	0.7	0.75	0.8
$u_{g,max}$ (cm/s)	11	14	33	47	63
$u_{g,min}$ (cm/s)	36	50	74	89	105
$u_{g,max} - u_{g,min}$	25	36	41	42	42
Experimental results from Khanna [24]					
$u_{g,max}$ (cm/s)	15	15	32	50	70
$u_{g,min}$ (cm/s)	33	48	63	80	93
$u_{g,max} - u_{g,min}$	18	33	31	30	23

$$\varepsilon = \frac{1 - \exp\{C_r[\exp(-\mathrm{NTU}) - 1]\}}{C_r}, \tag{36}$$

where NTU is calculated by

$$\mathrm{NTU} = \frac{UA}{C_{min}}, \tag{37}$$

where U is the overall heat transfer coefficient of the preheater including the internal and external convective heat transfer coefficients. Each node of the preheater tube is solved to find the outlet air temperature of the node. The outlet air temperature is used as the inlet air temperature for the next adjacent node of the preheater tube. The air temperature in the preheater is calculated at the boundary of two adjacent nodes and is given by

$$C_c[(T_{PH})_{i,j} - (T_{PH})_{i+1,j}] = \varepsilon C_{min}[(T_{\infty,PH})_{i,j} - (T_{\infty,PH})_{i,j-1}], \quad j = 1, \ldots, N_{RR}. \tag{38}$$

The temperature of the flue gas flow from each node, which is used as the ambient temperature for the radiation rods, is given by

$$C_h[(T_{\infty,PH})_{i,j} - (T_{\infty})_{i+1,j}] = \varepsilon C_{min}[(T_{\infty,PH})_{i,j} - (T_{PH})_{i,j-1}], \quad j = 1, \ldots, N_{RR}. \tag{39}$$

The algebraic equations governing the radiation rods and preheater are solved using the IMSL library.

The thermal efficiency of the burner is defined as the ratio of the radiation output to the target and the combustion heat and is defined by

$$\eta = \frac{Q_{rs}}{Q_{cb}}, \tag{40}$$

where the radiation output is given by

$$Q_{rs} = \sum(\varepsilon_r A_{rs}\sigma_{SB}T_{rs}^4 - \varepsilon_r A_t \sigma_{SB} T_t^4) \tag{41}$$

and the combustion heat is given by

$$Q_{cb} = \phi_a \left(\frac{\rho_{F,g}}{\rho_g}\right)_{stoich} \rho_g u_g H W \Delta h_{r,F}. \tag{42}$$

The convective heat transfer (Q_{RR} in Fig. 1(c)) between the radiation rods and the gas flow is calculated using the gas temperature based on the equivalence ratio (ϕ). The gas temperature is lower than the actual gas temperature based on the actual equivalence ratio (ϕ_a), which allows a conservative calculation of the heat extraction by the radiation rods. The equivalence ratio based on the actual fuel supply is calculated by

$$\phi_a = \frac{\phi}{1 - \eta}. \tag{43}$$

3. Results and discussion

3.1. Heat recirculation of superadiabatic radiant burner

The results of the numerical analysis for the conventional two-layer porous burner was compared and validated with the experimental results of Khanna [24]. It was found from the results of the numerical analysis that the flame speeds are in good agreement with the experimental results in Table 3.

The superadiabatic radiant burner with two-layer porous burner (PM1 and PM2), a preheater (PH) and radiation rods (RR) was analyzed. The temperature profiles of the superadiabatic radiant burner are depicted in Fig. 3(a). The conventional burner without preheater uses the inlet air at ambient temperature, while the superadiabatic burner uses an inlet air at higher temperatures because of the external heat recovery (preheating), and thus, expands the fuel lean limit of flammability. For the superadiabatic burner, the radiation rods made of a high thermal conductivity material are used to transfer the combustion heat efficiently from the flame to the radiating surface with a small temperature drop.

As a result of the preheating and separate heat transfer through the radiation rods, the temperature of the radiating surface is greater than the flue gas temperature and close to the adiabatic temperature. It is shown in Fig. 3(a) that, the radiating surface temperature is 81 K greater than that of the exit flue gas resulting in higher radiation efficiency. Note that the temperature at the interface of the porous media (between PM1 and PM2) was used as surrounding gas temperature of the fins of the radiation rods for the

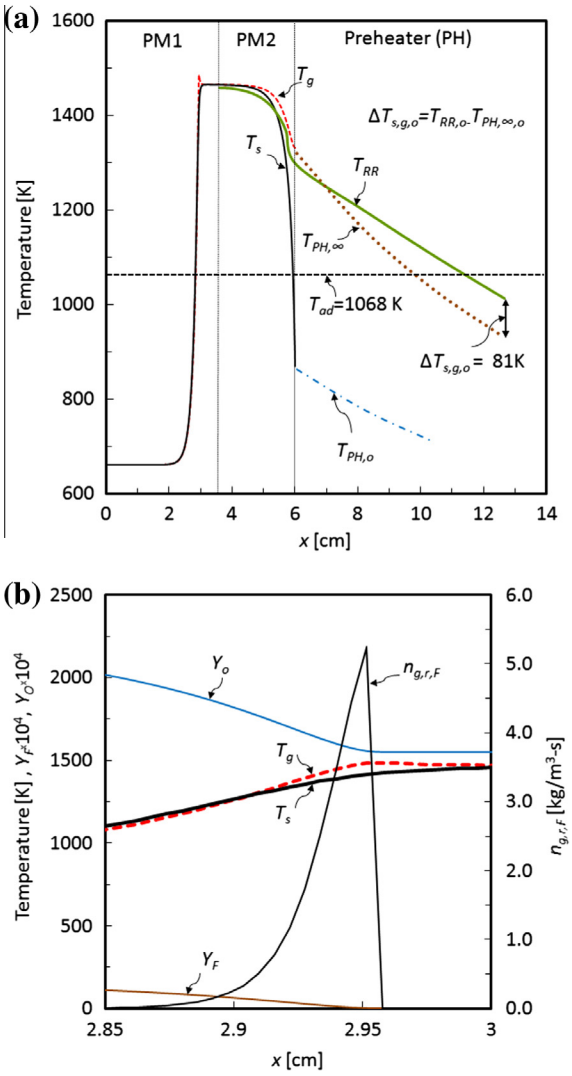

Fig. 3. (a) Temperature profiles of the superadiabatic burner. (b) Variations of the temperatures for the gas and solid phases, concentration of species and reaction rate in the porous media of the superadiabatic burner near the flame location (Φ_a = 0.5, Φ = 0.32, u_{air} = 6 cm/s).

convective heat transfer which is a more conservative way for the heat transfer calculation.

The temperature and gas species profiles in the upstream porous medium (PM1) near the flame location are magnified in Fig. 3(b). As shown in the figure, the gas temperature is slightly lower than the solid temperature near the inlet and then the gas temperature is higher than the solid temperature close to the flame. The heat transfer from the hotter solid to the incoming cold gas flow elucidates the internal heat recirculation which is in fact the heat transfer from the flame to the cold gas flow by solid matrix and is responsible for fuel-lean and superadiabatic combustion in the conventional porous burner [7,10,19]. After the flame, the thermal equilibrium between the gas and solid phases is quickly achieved due to the interfacial convection heat transfer. It is also shown in Fig. 3(b) that the fuel is completely depleted by the combustion, but the excess oxygen is still left under fuel-lean conditions.

The heat fluxes for the solid phase are shown in Fig. 4. The radiative, conductive and convective heat fluxes are given, respectively by

$$q_{rad} = \int_w^e \frac{\partial}{\partial x}\left(\varepsilon k_{s,r}\frac{\partial T_s}{\partial x}\right)dx = \left(\varepsilon k_{s,r}\frac{\partial T_s}{\partial x}\right)_e - \left(\varepsilon k_{s,r}\frac{\partial T_s}{\partial x}\right)_w, \tag{44}$$

$$q_{cd,s} = \int_w^e \frac{\partial}{\partial x}\left((1-\varepsilon)k_s\frac{\partial T_s}{\partial x}\right)dx = \left((1-\varepsilon)k_s\frac{\partial T_s}{\partial x}\right)_e - \left((1-\varepsilon)k_s\frac{\partial T_s}{\partial x}\right)_w, \tag{45}$$

$$q_{cv,s} = \int_w^e \left[\mathrm{Nu}_{D,p}\frac{k_g}{D_p}\left(\frac{A_{gs}}{V}\right)(T_g - T_s)\right]dx = \left[\mathrm{Nu}_{D,p}\frac{k_g}{D_p}\left(\frac{A_{gs}}{V}\right)(T_g - T_s)\right]_e - \left[\mathrm{Nu}_{D,p}\frac{k_g}{D_p}\left(\frac{A_{gs}}{V}\right)(T_g - T_s)\right]_w, \tag{46}$$

where the integral limits (e and w) denote the right (east) and left (west) faces of each node, respectively which are commonly used in the finite volume method. It is shown in Fig. 4 that all the heat fluxes are much greater near the flame and at the outlet region of the porous burner, resulting in non-thermal equilibrium between the solid and gas phases. The radiation and conduction heat transfers are balanced with the interfacial convection heat transfer, which is referred to as the aforementioned internal heat recirculation. The combustion reaction causes a sharp rise in the gas temperature and thus the positive convection heat transfer (heat gain from the gas phase). In the outlet region, the radiation heat transfer from the burner surface to the preheater decreases the solid temperature lower than the gas temperature resulting in the positive convective heat transfer.

The heat fluxes for the gas phase near the flame are shown in Fig. 5. The advective, conductive, convective, and combustion reaction heat fluxes are given by

$$q_{ad} = -\int_w^e \frac{\partial}{\partial x}\left[\varepsilon(\rho c_p u)_g\frac{\partial T_g}{\partial x}\right]dx = \left[\varepsilon(\rho c_p u)_g\frac{\partial T_g}{\partial x}\right]_e - \left[\varepsilon(\rho c_p u)_g\frac{\partial T_g}{\partial x}\right]_w, \tag{47}$$

$$q_{cd,g} = \int_w^e \frac{\partial}{\partial x}\left(k_{g,e}\frac{\partial T_g}{\partial x}\right)dx = \left(k_{g,e}\frac{\partial T_g}{\partial x}\right)_e - \left(k_{g,e}\frac{\partial T_g}{\partial x}\right)_w, \tag{48}$$

$$q_{cv,g} = -q_{cv,s} = \int_w^e \frac{\partial}{\partial x}\left[\mathrm{Nu}_{D,p}\frac{k_g}{D_p}\left(\frac{A_{gs}}{V}\right)(T_s - T_g)\right]dx = \left[\mathrm{Nu}_{D,p}\frac{k_g}{D_p}\left(\frac{A_{gs}}{V}\right)(T_s - T_g)\right]_e - \left[\mathrm{Nu}_{D,p}\frac{k_g}{D_p}\left(\frac{A_{gs}}{V}\right)(T_s - T_g)\right]_w, \tag{49}$$

$$q_{cb} = \int_w^e \frac{\partial}{\partial x}(\varepsilon\dot{n}_{g,r,F}\Delta h_{r,F})dx = (\varepsilon\dot{n}_{g,r,F}\Delta h_{r,F})_e - (\varepsilon\dot{n}_{g,r,F}\Delta h_{r,F})_w. \tag{50}$$

It is shown in Fig. 5 that the conduction heat transfer in the gas phase is dominant near the flame. It is also shown that the sign of the convective heat transfer is changed from positive (heat gain from the solid phase) to negative at the location where the gas phase temperature intersects with the solid phase temperature (Fig. 3(b)).

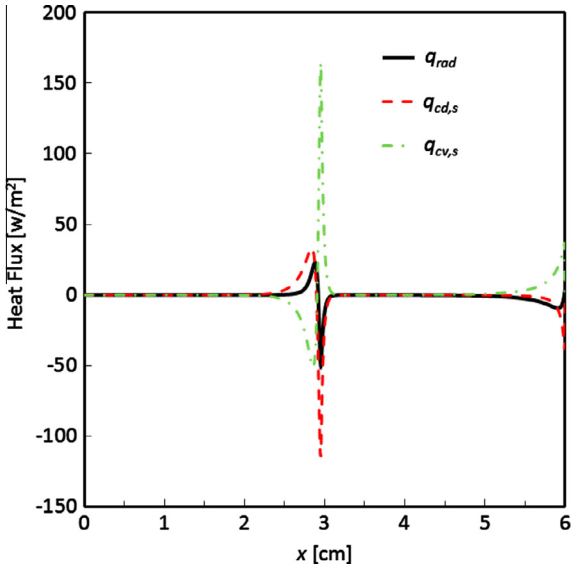

Fig. 4. Heat transfer components of the solid phase ($\Phi_a = 0.5$, $\Phi = 0.32$, $u_{air} = 6$ cm/s).

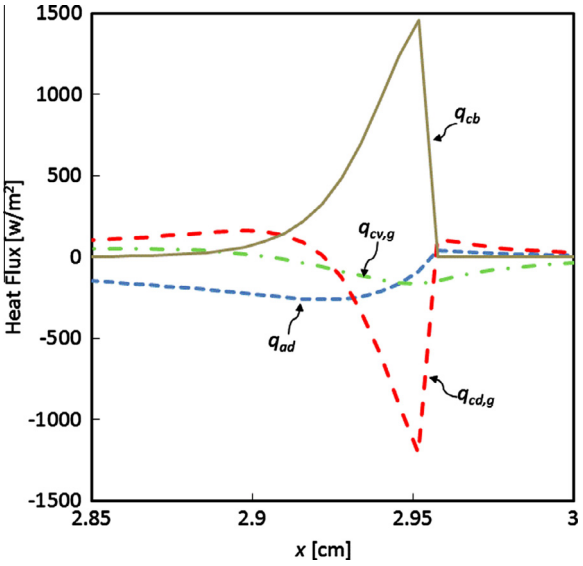

Fig. 5. The heat transfer components of the gas phase at the flame location ($\Phi_a = 0.5$, $\Phi = 0.32$, $u_{air} = 6$ cm/s).

3.2. Preheating of superadiabatic radient burner

The superadiabatic radiant burner combines the heat recovery by a preheater from the exit flue gas with the internal heat circulation in the porous burner. The external heat recovery (preheating) raises the inlet gas temperature and further expands the fuel lean flammability limit beyond that of the conventional porous burner.

The overall energy balance of the superadiabatic burner is given by

$$Q_{cb} = Q_{rs} + Q_{r,in} + Q_g, \tag{51}$$

where Q_{cb} is the combustion heat, Q_{rs} is the radiation output to the heating target, $Q_{r,in}$ is the radiation loss to the surrounding at the inlet and Q_g is the enthalpy loss by the flue gas and is given by

$$Q_g = Q_{g,o} - (Q_{g,in} + Q_{F,in}), \tag{52}$$

where $Q_{g,o}$ is the energy carried by the flue gas, $Q_{g,in}$ is the energy carried by the air into the preheater, and $Q_{F,in}$ is the energy carried by the fuel to the burner as shown in Fig. 1(c). Dividing Eq. (51) by Q_{cb}, the normalized energy balance is given by

$$1 = Q^*_{rs} + Q^*_{r,i} + Q^*_g. \tag{53}$$

Note that the normalized radiation output (Q^*_{rs}) is equal to the thermal efficiency (η) of the superadiabatic radiant burner. The normalized energy balance for the baseline condition (preheater air velocity u_{air} = 0.06 m/s) is shown in Fig. 6. It is shown in Fig. 6 that the largest portion of the combustion energy is lost by the flue gas. As the combustion heat input (equivalence ratio) is increased, the flame temperature and radiation output are increased. At the same time, the radiation loss is also increased because of the increased solid temperature at the burner inlet due to the preheated inlet gas temperature. But at high equivalence ratios (> 0.5), the radiation loss at the inlet is rapidly increased because of the high solid temperature of the burner at the inlet due to the flame proximity. It is also shown in Fig. 6 that the normalized heat recovery by the preheater (Q^*_{PH}) is decreased by increasing the equivalence ratio because the heat loss is increased. Note that the effectiveness of the preheater is decreased by increasing the equivalence ratio and ranges from 0.45 to 0.36.

The flame location in the upstream porous medium (PM1) for different preheating air velocities and equivalence ratios is depicted in Fig. 7. The preheating helps ignition of the fuel/air mixture especially at low equivalence ratios. The raised inlet gas temperature due to the preheating tends to draw the flame close to the inlet at low and high equivalence ratios. At intermediate equivalence ratios (0.4~0.51), the flame is located close to the interface of the porous media. Because the flame is far enough from the inlet of the burner, the burner temperature at the inlet ($T_{s,in}$) is close to the incoming gas temperature ($T_{g,in}$), and thus the radiation loss is rather minimal. At high equivalence ratios, however, the preheating draws the flame to the inlet and quickly raises the inlet burner temperature because of the proximity of the flame, and thus increases radiation loss resulting in decreased radiation output (Fig. 6).

Fig. 8 shows the gas temperatures at the location where the fins of the radiation rods are located. It is shown from the figure that as the preheater air velocity (combustion heat input) is increased, the gas temperature is rather slowly increased. This is also evidenced by the fact that the flame moves close to the burner inlet and more radiation is lost as the preheater air velocity is increased (Fig. 7). Note that the maximum solid temperatures of all data points in Fig. 8 are below 1600 K.

The thermal efficiencies of the superadiabatic radiant burner at various equivalence ratios and preheater air velocities are shown in Fig. 9. It is clearly shown that there is an optimum equivalence ratio around 0.5 regardless of preheater air velocity. The thermal efficiency is increased with the equivalence ratio until the flame moves to the burner inlet and thus more radiation loss occurs. It is also shown that the thermal efficiencies of the superadiabatic burner are significantly higher than that of the conventional burner [10] which is about 25%. This big improvement in the thermal efficiency attributes to the preheating by the flue gas and the efficient heat transfer through the radiation rods at a higher temperature than the flue gas.

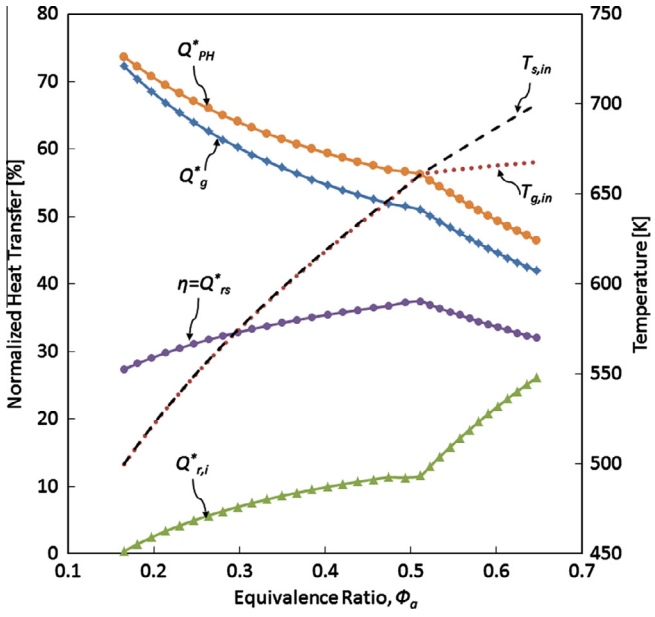

Fig. 6. Normalized energy balance and the inlet temperatures of the solid and gas phases of the superadiabatic burner for different fuel equivalence ratios (u_{air} = 6 cm/s).

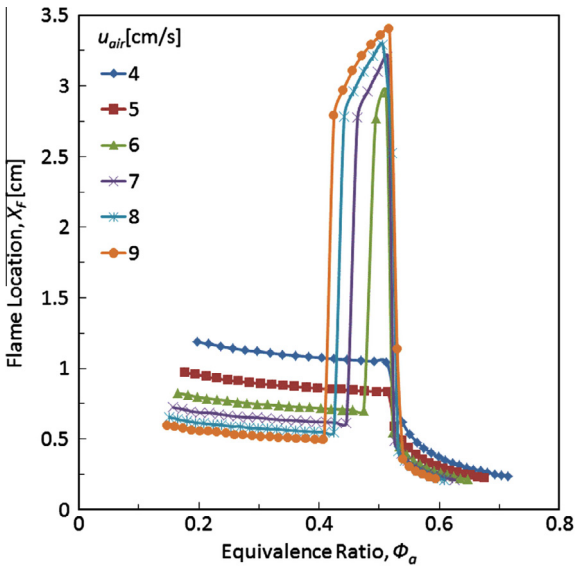

Fig. 7. Variation of flame location for different fuel equivalence ratios and preheater air velocities.

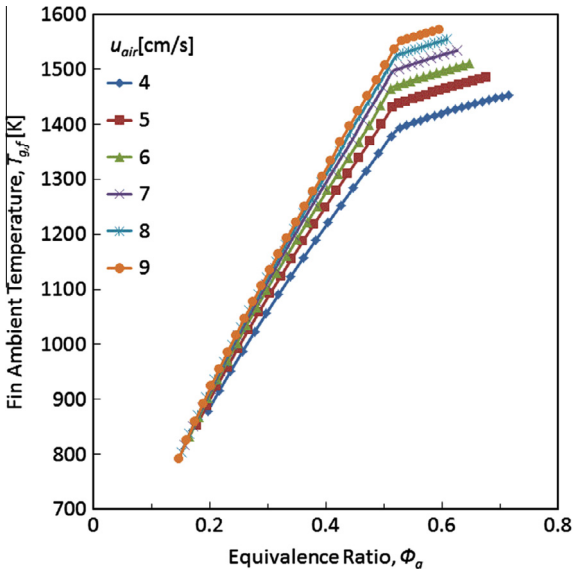

Fig. 8. Variation of ambient temperature of the fins of the radiation rods for different fuel equivalence ratios and preheater air velocities.

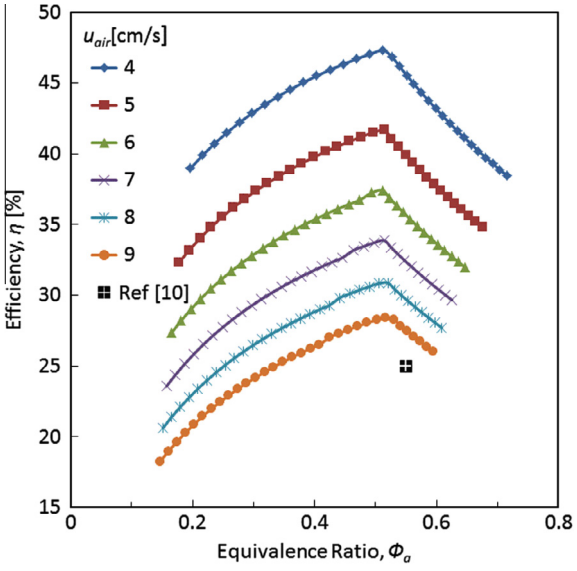

Fig. 9. Variation of the thermal efficiency with different fuel equivalence ratios and preheater air velocities.

4. Conclusions

A novel superadiabatic radiant porous burner using a preheater and radiation rods was presented and was numerically analyzed. The numerical results showed that thermal efficiency over 45% can be achieved. In the radiant burner, a preheater was used to externally recover the heat from the flue gas and increase the inlet air temperature so that the burner could operate at more fuel lean conditions than the conventional burners. The radiation rods, made of a metallic material (carbon steel) of high thermal conductivity, were used to transfer the combustion heat directly to the radiating surface at higher temperature than that of the flue gas. It was shown that combining the internal heat recirculation found in the conventional porous burners with the external heat recovery of the preheater and efficient heat transfer through the radiation corridors, allows the superadiabatic radiant burner to achieve higher radiating surface than the flue gas temperature and near the adiabatic flame temperature. As a result, a significant improvement in the thermal efficiency for the superadiabatic radiant burner is achieved as compared to the conventional porous burner.

Acknowledgement

Authors thank Professor Melik Sahraoui of Ecole Polytechnique de Tunisie for his valuable comments and suggestions for the initial phase of the numerical programming.

References

[1] Y. Yoshizawa, K. Sasaki, R. Echigo, Analytical study of the structure of radiation controlled flame, International Journal of Heat and Mass Transfer 31 (2) (1988) 311–319.
[2] T. Takeno, K. Sato, K. Hase, A theoretical study on an excess enthalpy flame, Symposium (International) on Combustion 18 (1) (1981) 465–472.
[3] K. Hanamura, R. Echigo, S.A. Zhdanok, Superadiabatic combustion in a porous medium, International Journal of Heat and Mass Transfer 36 (13) (1993) 3201–3209.
[4] V.S. Babkin, A.A. Korzhavin, V.A. Bunev, Propagation of premixed gaseous explosion flames in porous media, Combustion and Flame 87 (2) (1991) 182–190.
[5] K. Hanamura, R. Echigo, Thermal structure of superadiabatic combustion in porous media, in: Proceedings of KSME/JSME Thermal and Fluid, Engineering Conference, 1996, pp. 339–342.
[6] L.B. Younis, R. Viskanta, Experimental determination of the volumetric heat transfer coefficient between stream of air and ceramic foam, International Journal of Heat and Mass Transfer 36 (6) (1993) 1425–1434.
[7] B.P. Singh, M. Kaviany, Effect of solid conductivity on radiative heat transfer in packed beds, International Journal of Heat and Mass Transfer 37 (16) (1994) 2579–2583.
[8] F.A. Lammers, L.P.H. de Goey, A numerical study of flash back of laminar premixed flames in ceramic-foam surface burners, Combustion and Flame 133 (1–2) (2003) 47–61.
[9] M.T. Smucker, J.L. Ellzey, Computational and experimental study of atwo-section porous burner, Combustion Science and Technology 176 (8) (2004) 1171–1189.
[10] A.J. Barra, J.L. Ellzey, Heat recirculation and heat transfer in porous burners, Combustion and Flame 137 (1–2) (2004) 230–241.
[11] I. Schoegl, Radiation effects on flame stabilization on flat flame burners, Combustion and Flame 159 (9) (2012) 2817–2828.
[12] M. Sahraoui, M. Kaviany, Direct simulation vs volume-averaged treatment of adiabatic, premixed flame in a porous medium, International Journal of Heat and Mass Transfer 37 (18) (1994) 2817–2834.
[13] V. Bubnovich, M. Toledo, Analytical modelling of filtration combustion in inert porous media, Applied Thermal Engineering 27 (7) (2007) 1144–1149.
[14] J.-R. Shi, M.-Z. Xie, G. Li, H. Liu, J.-T. Liu, H.-T. Li, Approximate solutions of lean premixed combustion in porous media with reciprocating flow, International Journal of Heat and Mass Transfer 52 (3–4) (2009) 702–708.
[15] Y. Mahmoudi, M. Maerefat, Analytical investigation of heat transfer enhancement in a channel partially filled with a porous material under local thermal non-equilibrium condition, International Journal of Thermal Sciences 50 (12) (2011) 2386–2401.
[16] V. Bubnovich, M. Toledo, L. Henríquez, C. Rosas, J. Romero, Flame stabilization between two beds of alumina balls in a porous burner, Applied Thermal Engineering 30 (2–3) (2010) 92–95.
[17] S.C. Mishra, M. Steven, S. Nemoda, P. Talukdar, D. Trimis, F. Durst, Heat transfer analysis of a two-dimensional rectangular porous radiant burner, International Communications in Heat and Mass Transfer 33 (4) (2006) 467–474.
[18] Y. Huang, C.Y.H. Chao, P. Cheng, Effects of preheating and operation conditions on combustion in a porous medium, International Journal of Heat and Mass Transfer 45 (21) (2002) 4315–4324.
[19] K. Xu, M. Liu, P. Zhao, Stability of lean combustion in mini-scale porous media combustor with heat recuperation, Chemical Engineering and Processing: Process Intensification 50 (7) (2011) 608–613.
[20] C. Park, M. Kaviany, Combustion-thermoelectric tube, ASME Journal of Heat Transfer 122 (2000) 721–729.
[21] C. Park, M. Kaviany, Evaporation-combustion affected by in-cylinder, reciprocating porous-regenerator, ASME Journal of Heat Transfer 124 (2002) 184–194.
[22] M. Kaviany, Principles of Heat Transfer in Porous Media, Springer, New York, 1995.
[23] M. Kaviany, Essentials of Heat Transfer, Cambridge University Press, New York, 2011.
[24] V. Khanna, 1992, Experimental Analysis of Radiation for Methane Combustion within a Porous Medium Burner, M.S. thesis, University of Texas, Austin.
[25] T.L. Bergman, A.S. Lavine, F.P. Incropera, D.P. Dewitt, Fundamentals of Heat and Mass Transfer, John Wiley & Sons, Hoboken, 2011.